

# Three-Dimensional Representation of Geochemical Data from a Multidimensional Compositional Space

Pietro Armienti, Placido Longo

<sup>1</sup>*Dipartimento di Scienze della Terra, Università di Pisa, Pisa, Italy*

<sup>2</sup>*Dipartimento di Matematica Applicata, Università di Pisa, Pisa, Italy*

*E-mail: armienti@dst.unipi.it, p.longo@dma.unipi.it*

*Received January 2, 2011; revised May 3, 2011; accepted July 8, 2011*

## Abstract

Systems described by a wide set of variables, like rock compositions, may be often modeled by a reduced set of components, like minerals, that can be represented in diagrams in two or three dimensions. This paper deals with an original algorithm that allows the representation of compositional data in tetrahedral diagrams, provided that they can be recast on the basis of four end members. The algorithm is based on the orthogonal projection of a given point belonging to  $\mathbf{R}^n$  to the 3D-space through four  $\mathbf{R}^n$  points representing the compositions of suitable end members. The algorithm is applied to the assessment of mass balance problems (in weight% or molar basis) as well as to the identification of the geochemical imprint revealed by isotope ratios in igneous rock suites. The fields of possible applications are by far wider, encompassing all problems of comprehensive data representation from a multidimensional space to a bi-dimensional plot.

**Keywords:** Principal Component Analysis, Phase Diagrams, Rendering, Geochemistry

## 1. Introduction

Chemical composition of geologic systems (minerals, rocks, fluids, Earth reservoirs) may be described in terms of major and trace elements, as well as isotope ratios: a system may be thus represented by a set of  $n$  chemical variables corresponding to a point in the  $n$ -dimensional space. As a common practice, petrologists represent relations between geological systems (e.g. fractional crystallization or mixing processes) adopting 2D sections of the  $n$ -dimensional compositional space, as in Harker's diagrams.

3D diagrams are seldom used and, more commonly, relations among three compositional variables, recast to a constant sum (usually 1 or 100), are shown in triangular diagrams. The use of tetrahedral diagrams is limited, even if algorithms for a quick projection on the Cartesian plane have been already developed [1].

In systems with many components, compositions are often calculated in terms of end members: this is the case of minerals forming solid solutions, whose composition may be given as a mixture of the pure end members. A similar procedure is adopted in normative calculations that allow to recast the chemical analysis of a rock by fictive minerals. Similar approaches are adopted in ex-

perimental petrology when the chemical complexity of the systems is reduced to a small number of end members, suitable for representation in triangular or tetrahedral diagrams [2-4].

This paper focuses on a method to represent the composition of a system depending on a small number of end members defined by a given set of components. The case here discussed refers to a system in which four end members may form a suitable base for the compositional space, as in projections of petrologic interest or in isotopic systematic of OIB mantle reservoirs. It is worth to note that the a priori choice of four end members does not inhibit the possibility to represent additional phases: they will lay within the tetrahedron—as in the simplex approach [5]—if they are physical mixture of the end members; otherwise they will fall outside the tetrahedron if they are linear combinations of the end members with at least one negative tetrahedral coordinate. The scaling problems arising from the evaluation of Euclidean distance in multidimensional analysis performed through eigenvectors [6] does not induce biases in this method, since it uses the computation of the tetrahedral coordinates of each point which implies data normalization with respect to the values assumed by the end members at tetrahedron vertices.

## 2. The Algorithms

The code, the data sets, the figures and an introduction to Euclidean spaces are available for download at the address: [http://alan.dma.unipi.it/?page\\_id=1078](http://alan.dma.unipi.it/?page_id=1078).

### 2.1. Generalities

Assume that a system  $E$  is described in terms of  $n$  components (e.g. major elements): the  $n$ -tuple of values that define  $E$  can be thus considered as a vector of the  $n$ -dimensional space.

Considering  $\mathbf{A}$ ,  $\mathbf{B}$ ,  $\mathbf{C}$ ,  $\mathbf{D}$  as the vertices of a tetrahedron in  $\mathbf{R}^n$ , we want to find a set of relations representing a point  $\mathbf{E} \equiv (E_1, E_2, \dots, E_n)$  of  $n$ -dimensional space in terms of the four end members:

$$\begin{aligned} \mathbf{A} &\equiv (A_1, A_2, \dots, A_n) & \mathbf{B} &\equiv (B_1, B_2, \dots, B_n) \\ \mathbf{C} &\equiv (C_1, C_2, \dots, C_n) & \mathbf{D} &\equiv (D_1, D_2, \dots, D_n) \end{aligned}$$

To show the rationale of the procedure we start with the two end-member model of **Figure 1**. The end members  $\mathbf{A}$  and  $\mathbf{D}$  define the vector  $\mathbf{v}_1 = \mathbf{A} - \mathbf{D}$  and the projection  $\mathbf{E}^*$  of  $\mathbf{E}$  onto the straight line through  $\mathbf{A}$  and  $\mathbf{D}$  is obtained by :

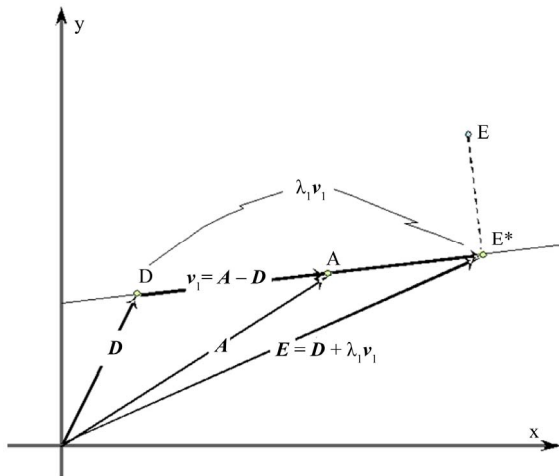


**Figure 1.** Exemplification in  $xy$ -plane of the projection method. The extremes of the segment  $AD$  represent the end-members and allow to define a map (orthogonal projection) of any point  $E$  to  $E^*$ , belonging to the line  $AD$ . The vector  $\mathbf{v}_1 = \mathbf{A} - \mathbf{D}$  and the projection  $\mathbf{E}^*$  of  $E$  to the straight line through  $\mathbf{A}$  and  $\mathbf{D}$  is obtained by  $\mathbf{E}^* = \mathbf{D} + \lambda_1 \mathbf{v}_1 = (1 - \lambda_1) \mathbf{D} + \lambda_1 \mathbf{A}$  where  $1 - \lambda_1$  and  $\lambda_1$  are the “two end-member” coordinates of  $\mathbf{E}^*$ . The coefficient  $\lambda_1$  is allowed to assume negative values to satisfy to the lever rule. For  $0 < \lambda_1 < 1$   $\mathbf{E}^*$  lays on the segment  $AD$ , is a convex combination of the two end members, and represents a physical mixture of them. If not, as in depicted case,  $\mathbf{E}^*$  still results from a linear combination of  $\mathbf{A}$  and  $\mathbf{D}$ : this guarantees the possibility of representing the projection of  $E$ , but claims for a different choice of end members to obtain  $\mathbf{E}^*$  as a physical mixture.

$$\mathbf{E}^* = \mathbf{D} + \lambda_1 \mathbf{v}_1 = (1 - \lambda_1) \mathbf{D} + \lambda_1 \mathbf{A}$$

where, according to the lever rule,  $1 - \lambda_1$  and  $\lambda_1$  are the “two end-member” coordinates of  $\mathbf{E}^*$ , equivalent to the tetrahedral coordinates in the case of four end-members. For  $0 < \lambda_1 < 1$   $\mathbf{E}^*$  lays on the segment  $AD$ , is a convex combination of the two end members, and represents a physical mixture of them. If not, as in **Figure 1**,  $\mathbf{E}^*$  still results from a linear combination of  $\mathbf{A}$  and  $\mathbf{D}$ : this guarantees the possibility of representing the projection of  $\mathbf{E}$ , but claims for a different choice of the end members to obtain  $\mathbf{E}^*$  as a physical mixture.

### 2.2. Anamorphosis: The Algorithm to Recast Analyses in Terms of End Members

In the case of four end members, the algorithm computes the orthogonal projection of the point  $\mathbf{E}^*$  in the 3D space through the end members, minimizing the  $n$ -dimensional Euclidean distance from the given point  $\mathbf{E}$  (see the file “Vectors\_in\_Euclidean\_Spaces.doc” at the data repository site [http://alan.dma.unipi.it/?page\\_id=1078](http://alan.dma.unipi.it/?page_id=1078) for generalities of the projection method in Euclidean space).

The steps of the algorithm are:

Given the tetrahedron vertices (the end members)  $\mathbf{A}$ ,  $\mathbf{B}$ ,  $\mathbf{C}$ ,  $\mathbf{D}$ ,  $\mathbf{R}^n$ , we compute vectors:

$$\mathbf{v}_1 = \mathbf{A} - \mathbf{D}, \mathbf{v}_2 = \mathbf{B} - \mathbf{D}, \mathbf{v}_3 = \mathbf{C} - \mathbf{D}$$

$$\text{Set } \alpha = \frac{\mathbf{v}_2 \cdot \mathbf{v}_1}{\|\mathbf{v}_1\|^2} \text{ and } \beta = \frac{\mathbf{v}_3 \cdot \mathbf{v}_1}{\|\mathbf{v}_1\|^2};$$

$$\mathbf{w}_1 = \mathbf{v}_1 \text{ and } \mathbf{w}_2 = \mathbf{v}_2 - \alpha \mathbf{w}_1$$

$$\text{Lastly, set } \gamma = \frac{\mathbf{v}_3 \cdot \mathbf{w}_2}{\|\mathbf{w}_2\|^2} \text{ and } \mathbf{w}_3 = \mathbf{v}_3 - \beta \mathbf{w}_1 - \gamma \mathbf{w}_2$$

-- For each point, we compute the vector  $\mathbf{E}' = \mathbf{E} - \mathbf{D}$  and its orthogonal projection  $\mathbf{E}''$  onto the subspace  $\langle \mathbf{w}_1, \mathbf{w}_2, \mathbf{w}_3 \rangle$ , that is  $\mathbf{E}'' = \lambda_1 \mathbf{w}_1 + \lambda_2 \mathbf{w}_2 + \lambda_3 \mathbf{w}_3$ .

$$\text{where } \lambda_i = \frac{\mathbf{E}' \cdot \mathbf{w}_i}{\|\mathbf{w}_i\|^2}, i = 1, 2, 3.$$

Recall that  $\mathbf{E}''$  is the linear combination of  $\mathbf{w}_1$ ,  $\mathbf{w}_2$ ,  $\mathbf{w}_3$  nearest to  $\mathbf{E}'$  in  $\mathbf{R}^n$ .

Since the distance is translation-invariant, it follows that  $\mathbf{E}^* = \mathbf{D} + \mathbf{E}'' = \mathbf{D} + \lambda_1 \mathbf{v}_1 + \lambda_2 \mathbf{v}_2 + \lambda_3 \mathbf{v}_3$  is the point in 3D passing through  $\mathbf{A}$ ,  $\mathbf{B}$ ,  $\mathbf{C}$ ,  $\mathbf{D}$  nearest to  $\mathbf{D} + \mathbf{E}' = \mathbf{E}$ .

Finally, we remark that

$$\begin{aligned} \mathbf{E}^* &= +\lambda_1 \mathbf{w}_1 + \lambda_2 \mathbf{w}_2 + \lambda_3 \mathbf{w}_3 = \mathbf{D} + \lambda_1 (\mathbf{A} - \mathbf{D}) \\ &+ \lambda_2 [\mathbf{B} - \mathbf{D} - \alpha (\mathbf{A} - \mathbf{D})] \\ &+ \lambda_3 \{ \mathbf{C} - \mathbf{D} - \beta (\mathbf{A} - \mathbf{D}) - \gamma [\mathbf{B} - \mathbf{D} - \alpha (\mathbf{A} - \mathbf{D})] \} \\ &= (\lambda_1 - \lambda_2 \alpha - \lambda_3 \beta + \lambda_3 \alpha \gamma) \mathbf{A} + (\lambda_2 - \lambda_3 \gamma) \mathbf{B} \\ &+ \lambda_3 \mathbf{C} + 1 - \lambda_1 - \lambda_2 - \lambda_3 + (\lambda_2 \alpha + \lambda_3 \beta + \lambda_3 \gamma - \lambda_3 \alpha \gamma) \mathbf{D} \end{aligned}$$

The sum of the four coefficients of the end members at the right hand of the above formula is 1; therefore, they represent the tetrahedral coordinates  $\tau_i$  of  $\mathbf{E}^*$  with respect to the four vertices  $\mathbf{A}, \mathbf{B}, \mathbf{C}, \mathbf{D}$ . Remark that if  $\lambda_1, \lambda_2, \lambda_3, \lambda_4 \geq 0$ , and  $\lambda_1, \lambda_2, \lambda_3, \lambda_4 \leq 1$ , the corresponding point lays *within* the tetrahedron with vertices  $\mathbf{A}, \mathbf{B}, \mathbf{C}, \mathbf{D}$ , represents a physical mixture of end members and the data set belongs to a *simplex* [5]. If some coefficient  $\lambda_i > 1$ , one or more coefficients have to attain negative values, due to the constant sum constraint, and the corresponding point has to lay *outside* the tetrahedron, requiring a different choice of the end members to express the data as physical mixtures.

The tetrahedral coordinates  $\tau_i$  are given by:

$$\begin{aligned} \tau_1 &= \lambda_1 - \lambda_2\alpha - \lambda_3\beta + \lambda_3\alpha\gamma \\ \tau_2 &= \lambda_2 - \lambda_3\gamma \\ \tau_3 &= \lambda_3 \\ \tau_4 &= 1 - \lambda_1 - \lambda_2 - \lambda_3 + \lambda_2\alpha + \lambda_3\beta + \lambda_3\gamma - \lambda_3\alpha\gamma \\ &= 1 - \tau_1 - \tau_2 - \tau_3 \end{aligned}$$

The point  $\mathbf{E}^*$  coincides with  $\mathbf{E}$  if and only if  $\mathbf{E}$  itself is a linear combination in  $\mathbf{R}^n$  of the end members with sum of coefficients equal to one (**Figure 1** shows the case when  $\mathbf{E}$  lays on the line through  $\mathbf{AD}$ ); otherwise,  $\mathbf{E}^*$  is distinct from  $\mathbf{E}$ , while enjoying the property to be at the minimal Euclidean distance from it, among all points of the (affine) subspace passing through the end members.

Let now  $(\mathbf{T}_1, \mathbf{T}_2, \mathbf{T}_3, \mathbf{T}_4)$  be the vectors in  $\mathbf{R}^3$  to which the tetrahedron vertices  $\mathbf{A}, \mathbf{B}, \mathbf{C}, \mathbf{D}$  are mapped on.

Finally,  $\mathbf{E}$  will be mapped in  $\mathbf{R}^3$  onto  $\mathbf{E}^{**}$  by the relation

$$\mathbf{E}^{**} = \tau_1 \mathbf{T}_1 + \tau_2 \mathbf{T}_2 + \tau_3 \mathbf{T}_3 + \tau_4 \mathbf{T}_4.$$

For a regular tetrahedron a possible choice is :

$$\begin{aligned} \mathbf{T}_1 &\equiv (0, 0, 1) & \mathbf{T}_2 &\equiv (2\sqrt{2/3}, 0, -1/3); \\ \mathbf{T}_3 &\equiv (-\sqrt{2/3}, \sqrt{2}/\sqrt{3}, -1/3) \\ \mathbf{T}_4 &\equiv (-\sqrt{2/3}, -\sqrt{2}/\sqrt{3}, -1/3) \end{aligned}$$

### 2.3. Tetra: The Algorithm to Plot Data in Rotating Tetrahedral Diagrams

The actual visualization requires a further mapping, namely a graphical projection from  $\mathbf{R}^3$  to the xy-plane, *i.e.* the computer screen. All the well known drawing maps, as Monge orthogonal, axonometric and perspective projections may work fine. We chose the vertical (orthogonal) projection on the  $YZ$  plane with a software that allows the user to choose the size, the type and the orientation of the tetrahedron. Moreover, animated rotation does provide a highly satisfactory perception of the

spatial distribution of data. Rotation is easily accomplished by using spherical coordinates, starting from a “canonical” orientation of the tetrahedron: set the centre in the origin of the axes and let the coordinates of vertex  $\mathbf{T}_1$  be  $(0,0,r)$ , while the edge  $\mathbf{T}_2 \mathbf{T}_3$  forms an angle  $\phi$  with the  $Y$  axis (**Figure 2**). It follows that the coordinates of  $\mathbf{B}$  are:

$$\begin{aligned} X_{T_2} &= r \sin(\alpha) \sin(\phi) \\ Y_{T_2} &= r \sin(\alpha) \cos(\phi) \\ Z_{T_2} &= r \cos(\alpha) \end{aligned}$$

where  $\alpha$  is the angle  $\mathbf{T}_1\mathbf{O}\mathbf{T}_2$ ; the coordinates of vertices  $\mathbf{T}_3$  e  $\mathbf{T}_4$  can be obtained from the above equations substituting  $\phi$  with  $(\phi + 2\pi/3)$  and  $(\phi + 4\pi/3)$  respectively. Varying  $\phi$  causes the tetrahedron to rotate around  $Z$  axis.

If tetrahedron is also allowed to rotate around the  $Y$  axis of an angle  $\theta$ , the new coordinates  $X'_i, Y'_i, Z'_i$  of each vertex are related to the old ones by the equations:

$$\begin{aligned} X'_i &= X_i \cos(\theta) + Z_i \sin(\theta) \\ Y'_i &= Y_i \\ Z'_i &= -X_i \sin(\theta) + Z_i \cos(\theta) \end{aligned}$$

The above equations show the dependence of the vertices  $(\mathbf{T}_1, \mathbf{T}_2, \mathbf{T}_3, \mathbf{T}_4)$  on  $\theta$  and  $\phi$ , and the relation :

$$\mathbf{E}^{**} = \tau_1 \mathbf{T}_1 + \tau_2 \mathbf{T}_2 + \tau_3 \mathbf{T}_3 + \tau_4 \mathbf{T}_4$$

allows to visualize the data set from different points of view. The animation is provided through step by step increments of  $\theta$  and  $\phi$  revealing possible clusters or special arrangements on planes or lines.

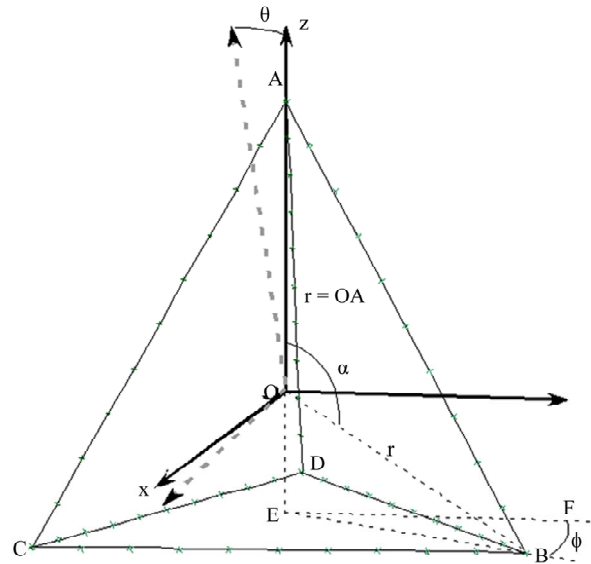


**Figure 2.** Canonical orientation of tetrahedral diagram used to plot data recast on the basis of four end members. The origin of the Cartesian axes is in the tetrahedron centre.

All the figures of this paper were produced with data and code that can be downloaded at the address: [http://alan.dma.unipi.it/?page\\_id=1078](http://alan.dma.unipi.it/?page_id=1078).

Animations exploit the features of tetrahedral diagrams at their best, showing 3D relationships among data arrays. You may observe that the above procedure maps the points of the tetrahedron **ABCD**, which maybe highly irregular, onto those of the regular one **T<sub>1</sub>, T<sub>2</sub>, T<sub>3</sub>, T<sub>4</sub>**.

This provides a normalization in the representation of the data, since the position of the plotted points in the regular tetrahedron does not depend upon the absolute magnitude of the scalars used in the original data set. This means that if we use components such as different trace elements, whose abundances span from a few ppm - like Nd - to thousands of ppm - like Sr -, there is no need of scaling the data to some common order of magnitude.

### 3. Some Applications

#### 3.1. Mass Balance. Case 1

**Figure 3** shows two sets of points, computed by adding different amounts of olivine, clinopyroxene and plagioclase to a lava from Mt Etna. The minerals and the lava were assumed to be the end members for the tetrahedral diagram. Minerals. The points were calculated keeping constant the amount of pyroxene (30% and 70%) and adding to the lava regularly increasing amounts of the other two phases to simulate cumulus processes. The cumulate compositions were assessed with the mass balance equation

$$P_i = \frac{I_i + \sum_{j=1}^n a_{ij} x_j}{100 + \sum_{j=1}^n x_j}$$

where:

$P_i$  is the wt% of the component  $i$  in the cumulate

$I_i$  is its amount in wt% in the lava

$a_{ij}$  is its weight fraction in phase  $j$

$x_j$  is the weight fraction of phase  $j$  in the cumulate.

Each cumulitic composition was then plotted in the tetrahedral diagram. The solids are represented in **Figure 3** by the points laying on the OL-CPX-PLG face; the compositions resulting by the additions of the solids to the lava lay on lines joining the lava vertex with the solid towards the base (see the regular arrays of points in **Figure 3**). The representation is consistent with the expected mass ratio assumed in the data generation.

For comparison, **Figure 3** shows the analyses of lavas emitted by Mt Etna from 1971 to 2002 [7]. These data lay outside the tetrahedron since they were originated by

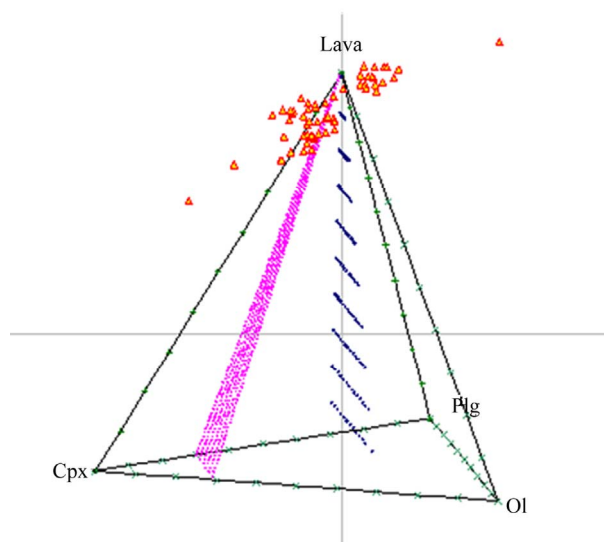


**Figure 3.** The coordinates of the point arrays were calculated in  $R^n$  by using the equation.  $P_i^{AB} = A_i + (A_i - B_i) * \Delta$ . The tetrahedron orientation is  $\phi = 51$ ,  $\theta = 12$ .

a mechanisms different from cumulus or fractionation. The adoption of negative tetrahedral coordinates still allows to represent data outside the tetrahedron in terms of linear combination of the four end members and suggests that it is possible to choose a different set of end members to plot data within the tetrahedron.

#### 3.2. Mass Balance. Case 2

Reporting compositional data as molar fractions provides diagrams that account for the molecular proportions of minerals chosen as end members. An example is shown in **Figure 4(a)**, reporting the expanded normative basalt tetrahedron (Larnite, Nepheline, Fosterite, Quartz - La, Ne, Fo, Q) [4,8] where normative minerals are given as molecular fractions and then projected within the tetrahedron. Data are mineral and whole rock analyses of a suite of pyroxenites from North Victoria Land (Antarctica) [9]. The petrogenetic hypothesis that pyroxenites are a physical mixture of their minerals is easily checked, as well as it is plainly evident from top and middle projection where data are shown with different orientations in the La, Ne, Fo, Q projection.

In the bottom diagram the same data are recalculated in terms of the Di, Ne, Fo, Q. The hypothesis is confirmed and the clinopyroxenes, as expected, are grouped towards the Di vertex.

Molecular proportions of rock analyses may be recast following the procedure of O'Hara [3] to obtain CMAS components. By adopting pure components as end members (figures in bold), we obtain the classical CMAS projection (**Figure 4**, bottom). Projections can be made

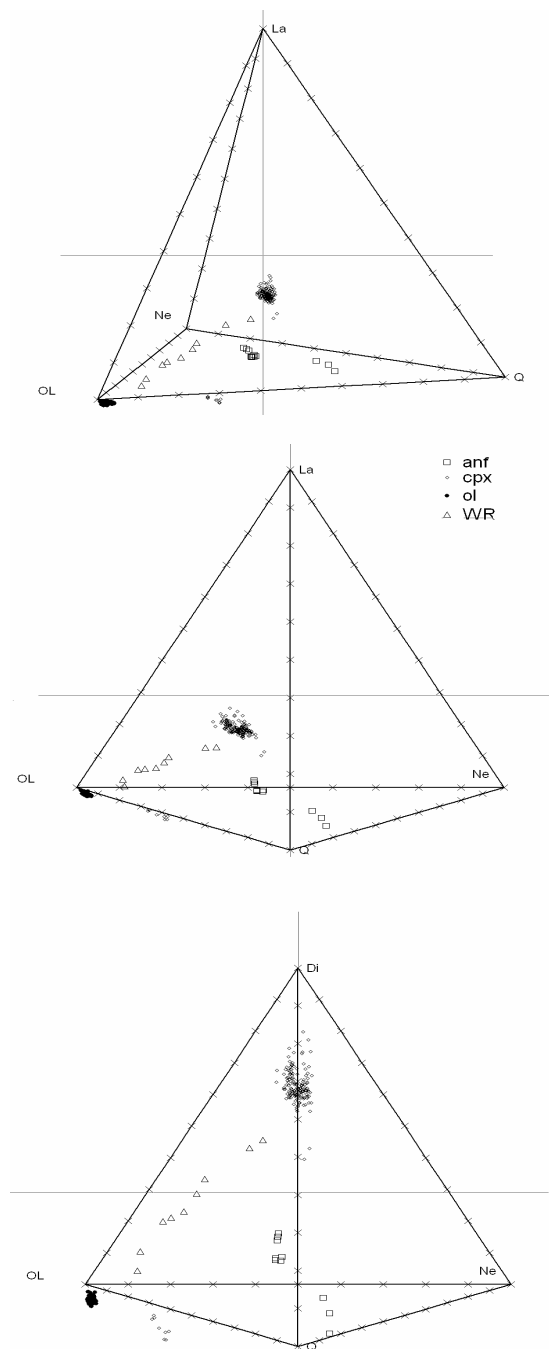


**Figure 4. TOP and MIDDLE:** two different orientations of expanded normative tetrahedron La-Ne-Q-Ol [4,10]. Normative minerals are recalculated on a molecular basis (Table 2) and then projected within the tetrahedron through the algorithm *anamorphosis*. The diagrams show a set of pyroxenites and their minerals [13], with major element oxides recast as molar fractions. **BOTTOM:** The same data set with a different choice of end-members. Note the displacement of clinopyroxenes from the centre of the tetrahedron (the position of diopside in tetrahedron La-Ne-Q-Ol) toward the top vertex, representing the diopside end-member in the new projection. The tetrahedron orientation is  $\phi = 0, \theta = 12$ .

on a molar basis or on a weight basis if molecular proportions or molecular weights are provided.

The same data set can be easily recast according to a subset of components within the CMAS, providing the compositions of the new end members in the CMAS system. For a projection in the system Q-Ol-CaTs-Di Q = S, Ol =  $M_2S$ , CaTs = CAS, Di =  $CMS_2$  (Figure 4, bottom), a weight or a molecular projection are obtained by the following matrices.

	C	M	A	S
Q	0	0	0	1 SiO <sub>2</sub>
OL	0	2/3 MgO	0	1/3 SiO <sub>2</sub>
CaTs	1/3 CaO	0	1/3 Al <sub>2</sub> O <sub>3</sub>	1/3 SiO <sub>2</sub>
Di	1/4 CaO	1/4 MgO	0	2/4 SiO <sub>2</sub>
Molecular Proportions				
	C	M	A	S
Q	0	0	0	1
OL	0	2/3	0	2/3
CaTs	1/3	0	1/3	1/3
Di	1/4	1/4	0	2/4
Molecular Weights				
	C	M	A	S
Q	0	0	0	60.09
OL	0	26.69	0	20.03
CaTs	18.69	0	33.99	20.00
Di	14.02	10.01	0	30.45

Allowing for negative values of tetrahedral coordinates, Nepheline may be computed in terms of CMAS components as  $Ne = C_{2/3}A_{2/3}S_{-1/3}$ . This permits projections within the CMAS of Ne-bearing systems on both molecular or weight basis (Figure 4):

	C	M	A	S
Pl	1/4 CaO	0	1/4 Al <sub>2</sub> O <sub>3</sub>	2/4 SiO <sub>2</sub>
Ol	0	2/3 MgO	0	1/3 SiO <sub>2</sub>
Di	1/4 CaO	1/4 MgO	0	2/4 SiO <sub>2</sub>
Ne	2/3 CaO	0	2/3 Al <sub>2</sub> O <sub>3</sub>	-1/3 SiO <sub>2</sub>
Molecular Proportions				
	C	M	A	S
Pl	1/4	0	1/4	2/4
Ol	0	2/3	0	1/3
Di	1/4	1/4	0	2/4
Ne	2/3	0	2/3	-1/3
Molecular Weights				
	C	M	A	S
Pl	14.02	0	25.49	30.04
Ol	0	26.69	0	20.03
Di	14.02	10.01	0	30.45
Ne	37.39	0	67.97	-20.03

**Table 2** allows an easy calculations for a large set of normative minerals.

### 3.3. Mantle Reservoirs

In spite of the growing evidence of widespread heterogeneities in the mantle [10-12], the isotopic composition of oceanic basalts is commonly described in terms of four main mantle sources, of which basalts keep the isotopic composition and characteristic ratios of incompatible elements [13,14]. The main mantle reservoirs involved in the genesis of Oceanic Islands Basalts (OIB) are considered to be: the depleted asthenospheric mantle (DMM), the common source usually found in oceanic

islands (OIB-HIMU) with a relatively large U/Pb ratio, and the two enriched components, namely the Enriched Mantle I (EMI) and the Enriched Mantle II (EMII). Reference values of isotopic ratios of Sr, Nd, Pb are shown in **Table 3**.

An overview of OIB compositions in the 3D space, defined by the isotopic ratios  $^{87}\text{Sr}/^{86}\text{Sr}$ ,  $^{206}\text{Pb}/^{204}\text{Pb}$ ,  $^{143}\text{Nd}/^{144}\text{Nd}$ , led Hart [8] to the conclusion that most of oceanic island basalts lay within a tetrahedron defined by the four vertices EMI, EMII, DMM and HIMU. We tested our model assuming that the same holds in n-dimensional space. In **Figure 5** a plot of basalts from Hawaii, Galapagos and Cook islands is shown. Data have been obtained from the GEOROC database.

**Table 1. Compositions of end members adopted to represent data in Figure 3.**

	SiO <sub>2</sub>	TiO <sub>2</sub>	Al <sub>2</sub> O <sub>3</sub>	FeO	MnO	MgO	CaO	Na <sub>2</sub> O	K <sub>2</sub> O	P <sub>2</sub> O <sub>5</sub>
Lava	47.1	1.85	17.85	10.4	0.2	5.54	11.32	3.47	1.86	0.4
OI	40.28	0	0	10.561	0.16	49.03	0.2775	0	0	0
CPX	51.78	0.504	2.91	4.86	0.22	16.36	22.432	0.249	0.243	0
PLG	48.96	0	32.5	0.5	0	0	15.04	2.64	0	0

**Table 2. Molecular composition of minerals in the Expanded Basalt Tetrahedron of Figure 4. End members in bold.**

			SiO <sub>2</sub>	Al <sub>2</sub> O <sub>3</sub>	TiO <sub>2</sub>	FeO	MnO	MgO	CaO	Na <sub>2</sub> O	K <sub>2</sub> O	P <sub>2</sub> O <sub>5</sub>
<b>La</b>	Ca <sub>2</sub> SiO <sub>4</sub>	<i>Larnite</i>	0.33	0.00	0.00	0.00	0.00	0.00	0.67	0.00	0.00	0.00
Ra	Ca <sub>3</sub> Si <sub>2</sub> O <sub>7</sub>	<i>Rankinite</i>	0.40	0.00	0.00	0.00	0.00	0.00	0.60	0.00	0.00	0.00
Mer	Ca <sub>3</sub> MgSi <sub>2</sub> O <sub>8</sub>	<i>Merwinite</i>	0.33	0.00	0.00	0.00	0.00	0.17	0.50	0.00	0.00	0.00
Wo	CaSiO <sub>3</sub>	<i>Wollastonite</i>	0.50	0.00	0.00	0.00	0.00	0.00	0.50	0.00	0.00	0.00
<b>Fo</b>	Mg <sub>2</sub> SiO <sub>4</sub>	<i>Forsterite</i>	0.33	0.00	0.00	0.00	0.00	0.67	0.00	0.00	0.00	0.00
<b>Ne</b>	NaAlSiO <sub>4</sub>	<i>Nefelina</i>	0.33	0.33	0.00	0.00	0.00	0.00	0.00	0.33	0.00	0.00
<b>Qtz</b>	SiO <sub>2</sub>	<i>Quarzo</i>	1.00	0.00	0.00	0.00	0.00	0.00	0.00	0.00	0.00	0.00
En	MgSiO <sub>3</sub>	<i>Enstatite</i>	0.50	0.00	0.00	0.00	0.00	0.50	0.00	0.00	0.00	0.00
Ab	NaAlSi <sub>3</sub> O <sub>8</sub>	<i>Albite</i>	0.60	0.20	0.00	0.00	0.00	0.00	0.00	0.20	0.00	0.00
Di	CaMgSi <sub>2</sub> O <sub>6</sub>	<i>Diopside</i>	0.50	0.00	0.00	0.00	0.00	0.25	0.25	0.00	0.00	0.00
Ak	Ca <sub>2</sub> MgSi <sub>2</sub> O <sub>7</sub>	<i>Akermanite</i>	0.40	0.00	0.00	0.00	0.00	0.20	0.40	0.00	0.00	0.00

**Table 3. Values of mantle components adopted for projection of data in Figure 5.**

#### Figure 5(a)-(b).

	$^{87}\text{Sr}/^{86}\text{Sr}$	$^{206}\text{Pb}/^{204}\text{Pb}$	$^{207}\text{Pb}/^{204}\text{Pb}$	$^{208}\text{Pb}/^{204}\text{Pb}$	$^{143}\text{Nd}/^{144}\text{Nd}$	Ref.
DMM	0.70300	18.500	15.450	38.040	0.51320	[15]
EM I	0.70530	17.600	15.470	37.961	0.51120	[15]
EM II	0.72200	18.590	15.620	39.000	0.51265	[15]
HIMU	0.70228	21.690	15.710	40.734	0.51285	[16]

#### Figure 5(c)-(d).

	$^{87}\text{Sr}/^{86}\text{Sr}$	$^{206}\text{Pb}/^{204}\text{Pb}$	$^{207}\text{Pb}/^{204}\text{Pb}$	$^{208}\text{Pb}/^{204}\text{Pb}$	$^{143}\text{Nd}/^{144}\text{Nd}$	Ref.
DMM	0.70241	18.106	15.441	38.040	0.51320	this work
EM I	0.70507	17.535	15.461	37.960	0.51232	this work
EM II	0.72200	18.590	15.620	39.000	0.51265	[15]
HIMU	0.70283	21.612	15.828	40.734	0.51280	[10]

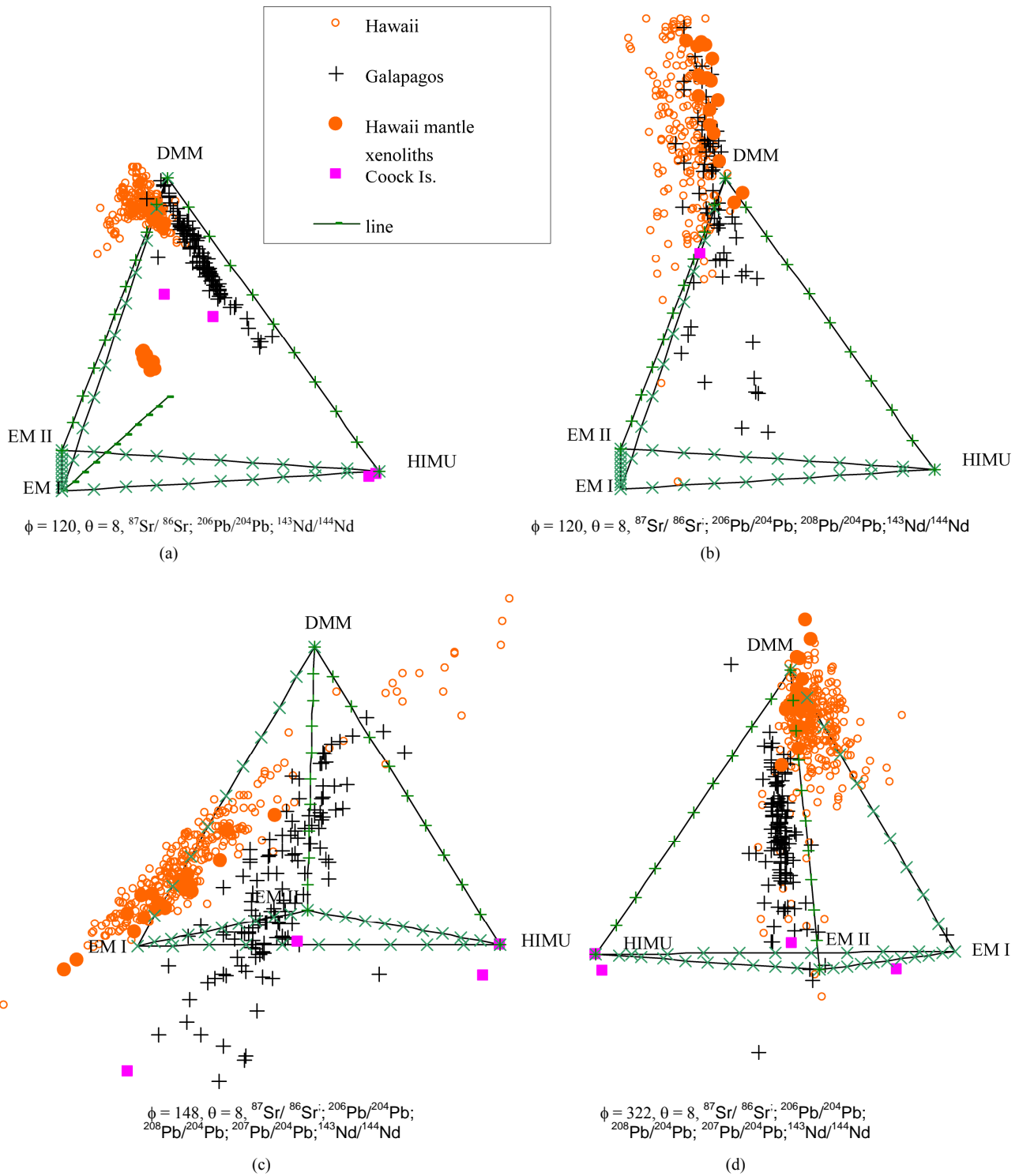


Figure 5. (a) Three isotope ratios ( ${}^{87}\text{Sr}/{}^{86}\text{Sr}$ ,  ${}^{206}\text{Pb}/{}^{204}\text{Pb}$ ,  ${}^{143}\text{Nd}/{}^{144}\text{Nd}$ ) were used to define mantle components and plot Hawaii, Galapagos and Cook Islands basalts and Hawaii mantle xenoliths. (b) The same data set were plotted using the same tetrahedron orientation but using five isotope compositions ( ${}^{87}\text{Sr}/{}^{86}\text{Sr}$ ,  ${}^{206}\text{Pb}/{}^{204}\text{Pb}$ ,  ${}^{207}\text{Pb}/{}^{204}\text{Pb}$ ,  ${}^{208}\text{Pb}/{}^{204}\text{Pb}$ ,  ${}^{143}\text{Nd}/{}^{144}\text{Nd}$ ) to define the HIMU, DMM, EMI and EM II mantle. Data still group in well distinct arrays that can be put in evidence by a suitable choice of  $\phi$  and  $\theta$ . Values of isotope ratios of mantle components are reported in Table 3, upper part. (c), (d) A different choice for isotope compositions of mantle components and tetrahedron orientation allows to get a better representation of regular arrays defined by the data sets. Values adopted for the end members are given in the second part of table 3. Basalt data from the GEOROC data base.

Diagram of **Figure 5(a)** reveals that points form different clusters in the tetrahedron for the two archipelagos. Some of the Cook Islands data fall just on the HIMU

component and all data sets appear to point towards the HIMU component (**Figure 5(a)**). In particular, it is possible to observe a branch of the Hawaii data set directed towards an enriched component **Figure 5(d)**, while harzburgite mantle xenoliths show an evident imprint of an EM I end member.

Both Hawaii and Galapagos are widely recognized as plume-related island chains; thus a plume HIMU component should appear to mix with asthenospheric mantle in both island chains, as it results from **Figure 5(a)**, obtained using tree isotopic ratios.

However, this plotting method may be used to represent the same data set adopting a larger number of independent components, as in **Figure 5(b)-(d)**. The end members are still defined as HIMU; DMM, EM I and EM II but using five components ( $^{87}\text{Sr}/^{86}\text{Sr}$ ,  $^{206}\text{Pb}/^{204}\text{Pb}$ ,  $^{207}\text{Pb}/^{204}\text{Pb}$ ,  $^{208}\text{Pb}/^{204}\text{Pb}$ ,  $^{143}\text{Nd}/^{144}\text{Nd}$ ) to plot the same data set. This allows to observe a different point arrangements: each data set keeps a well distinct trend in every diagram, but tends to form more dispersed clusters, due to a larger number of components used to define end members. A different choice for isotopic compositions of mantle components and tetrahedron orientation may allow to get a better representation of regular arrays in the data sets (**Figure 5(c)** and **(d)**). Hawaii data suggest the mixing between two mantle components, while a plane arrangement suggests that the mixing of three mantle components is needed to produce Galapagos basalts. Values adopted for the new end members are given in the second part of **Table 3**.

A suitable choice of end members,  $\phi$  and  $\theta$  allows to recognize a typical compositional imprint for each mantle region, in spite of the starting hypothesis of a common HIMU source depicted in **Figure 5(a)**.

A detailed interpretation of petrogenetic hypotheses is beyond the purposes of this paper. However, it is evident how our approach allows an insight, into data sets, deeper than the simple diagrams in which two isotopic ratios only are adopted.

#### 4. Conclusions

Our method provides a useful and general way to visualize, in three-dimensional diagrams, data sets characterized by a high number of components. Data are orthogonally projected from the Euclidean space  $\mathbf{R}^n$  to the three-dimensional subspace of  $\mathbf{R}^n$  passing through four suitable end members, previously chosen. The method evaluates the tetrahedral coordinates, allowing to map any point in  $\mathbf{R}^n$  to the  $\mathbf{R}^3$  point with the same tetra-

hedral coordinates, obtaining a distorted map (*anamorphosis*) of a perhaps highly irregular tetrahedron in  $\mathbf{R}^n$  into a regular tetrahedron in  $\mathbf{R}^3$ . This procedure ensures normalization of data and allows to use components whose numerical values may differ in the order of magnitude.

End member physical mixtures (*convex* combinations) are represented by points *within* the tetrahedron and the methods developed for the study of “constant sum” sets [5,8] may be applied for the interpretation of data. However, our projection method also allows the representation of natural compositions laying *outside* the  $\mathbf{R}^n$  tetrahedron as *linear* (non convex) combinations of the end members, plotting them outside the 3D tetrahedron. If these points fall far from the tetrahedron, a different choice of end members may be accomplished to find a tetrahedron containing them.

A final projection from  $\mathbf{R}^3$  to the graphic plane plots the diagram; suitable orientation of the tetrahedron in the plot reveals 1D and 2D arrays, corresponding to binary or ternary mixtures. Animated rotation of the diagram may be easily obtained and allows a fast and effective overview of data sets. The use of mineral and rock analyses to define end members ensures the possibility of the geometrical solution of mass balance problems. The obvious application of this kind of plots may be found in experimental petrology for the representation of compositions of complex systems like the normative Basalt tetrahedron or the CMAS system, computed on a weight% or molecular basis. This kind of projections also allows to explore multidimensional data sets, like those characterizing the isotope systematic of magmas and their incompatible element ratios.

#### 5. References

- [1] P. Armienti, “TETRASEZ an Interactive Program in BASIC to Perform Tetrahedral Diagrams,” *Computer & Geosciences*, Vol. 12, No. 2, 1986, pp. 229-241. [doi:10.1016/0098-3004\(86\)90010-5](https://doi.org/10.1016/0098-3004(86)90010-5)
- [2] R. O. Sack, D. C. Walker and I. S. E. Carmichael, “Experimental Petrology of Alkalic Lavas: Constraints on Cotectics of Multiple Saturation in Natural Basic Liquids,” *Contributions to Mineralogy and Petrology*, Vol. 96, No. 1, 1987, pp. 1-23. [doi:10.1007/BF00375521](https://doi.org/10.1007/BF00375521)
- [3] M. J. O’Hara, “The Bearing of Phase Equilibria Studies on the Origin and Evolution of Basic and Ultrabasic Rocks,” *Earth-Science Reviews*, Vol. 4, 1968, pp. 69-133. [doi:10.1016/0012-8252\(68\)90147-5](https://doi.org/10.1016/0012-8252(68)90147-5)
- [4] H. S. J. Yoder and C. E. Tilley, “Origin of Basalt Magma: An Experimental Study of Natural and Synthetic Rock Systems,” *Journal of Petrology*, Vol. 3, No. 3, 1962, pp. 342-532.
- [5] J. Aitchison, “The Statistical Analysis of Compositional

- Data,” Chapman and Hall, London, 1986, p. 416.
- [6] C. J. Allègre, B. Hamelin, A. Provost and B. Dupré, “Topology of Isotopic Multispace and Origin of Mantle Chemical Heterogeneities,” *Earth and Planetary Science Letters*, Vol. 81, 1986, pp. 319-337.
- [7] P. Armienti, S. Tonarini, F. Innocenti and M. D’Orazio, “Mount Etna Pyroxene as Tracer of Petrogenetic Processes and Dynamics of the Feeding System,” In: L. Becaluva, G. Bianchini, M. Wilson, Eds., *Volcanism in the Mediterranean and Surrounding Regions*, Geological Society of America, Special Paper, Vol. 418, 2007, pp. 265-276.
- [8] J. F. Schairer and H. S. Yoder Jr., “Crystal and Liquid Trends in Simplified Alkali Basalts,” *Carnegie Institution of Washington*, Vol. 63, 1964, pp. 65-75.
- [9] C. Perinelli, P. Armienti and L. Dallai, “Thermal Evolution of the Lithosphere in a Rift Environment as Inferred from the Geochemistry of Mantle Cumulates. Northern Victoria Land, Antarctica,” *Journal of Petrology*, Vol. 52, No. 4, 2011, pp. 665-690.  
[doi:10.1093/petrology/egq099](https://doi.org/10.1093/petrology/egq099)
- [10] S. Hart, E. H. Hauri, L. A. Oschmann and J. A. Whitehead, “Mantle Plumes and Entrainment: Isotopic Evidence,” *Science*, Vol. 256, No. 5056, 1992, pp. 517-520.  
[doi:10.1126/science.256.5056.517](https://doi.org/10.1126/science.256.5056.517)
- [11] E. Hauri and S. R. Hart, “Rhenium Abundances and Systematics in Oceanic Basalts,” *Chemical Geology*, Vol. 13, No. 1-4, 1997, pp. 185-205.  
[doi:10.1016/S0009-2541\(97\)00035-1](https://doi.org/10.1016/S0009-2541(97)00035-1)
- [12] P. Armienti and D. Gasperini, “Do We Really Need Mantle Components to Define Mantle Composition?” *Journal of Petrology*, Vol. 48, No. 4, 2007, pp. 693-709.  
[doi:10.1093/petrology/egl078](https://doi.org/10.1093/petrology/egl078)
- [13] J. A. Martin-Fernández, C. Barcelò-Vidal and V. Pawlowsky-Glahn, “Dealing with Zeros and Missing Values in Compositional Data Sets Using Nonparametric Imputation,” *Mathematical Geology*, Vol. 35, No. 3, 2003, pp. 45-54.
- [14] S. S. Sun and W. F. McDonough, “Chemical and Isotopic Systematics of Oceanic Basalts: Implications for Mantle Composition and Processes,” In: A. D. Saunders and M. J. Norry, Eds., *Magmatism in Ocean Basins*, Geological Society Special Publication, London, 1989, pp. 313-345.
- [15] A. D. Saunders, M. J. Norry and J. Tarney, “Origin of MORB and Chemically Depleted Mantle Reservoirs: Trace Element Constraints,” *Journal of Petrology*, Vol. 1, No. 1, 1988, pp. 414-445.
- [16] D. J. Chaffey, R. A. Cliff and B. M. Wilson, “Characterization of the St. Helena Magma Source,” In: A. D. Saunders and M. J. Norry Eds., *Magmatism in Ocean Basins*, Geological Society Special Publication, London, Vol. 42, 1989, pp. 257-276.